Understanding the Mechanism of Solvent-Mediated Adhesion of Vacuum Deposited Au and Pt Thin Films onto PMMA Substrates

*Alan K. Mo, Victoria L. Brown, Brandon K. Rugg, Thomas C. DeVore, Harry M. Meyer, Xiaofeng Hu, W. Christopher Hughes, and Brian H. Augustine**

The adhesion of vapor deposited Au and Pt thin films onto poly(methyl methacrylate) (PMMA) substrates can be significantly enhanced by either spin-casting or vapor-exposure to hydrohalocarbon solvents prior to metal deposition. X-ray photoelectron spectroscopy (XPS) and evolved gas analysis Fourier transform infrared spectroscopy detect residual halogenated solvent at the PMMA surface which chemically activates the surface. Density functional theory (DFT) calculations show that the solvent molecules form a Lewis acid-base adduct with the ester oxygens in PMMA. DFT predicts that the deposited metal atom (M) inserts into the C–halogen (X) bond on either $CHCl_3$ or $CHBr_3$ to form a O–M–X interaction. This is consistent with M–X bonding observed in high resolution XPS. A model is proposed in which the bond energy of the C–X bond of the solvent must be weak enough so that it can be cleaved by the metal atom to form a M–X bond. A negative control of PMMA exposed to CHF_3 is shown to have no effect on Au or Pt adhesion since the bond dissociation energy of the C–F bond is stronger than the C–Cl and C–Br bond energy compared to the metal halide bond energies.

1. Introduction

The deposition of metal thin films onto polymeric substrates is a critical processing step in a variety of processes used in the automotive, aerospace, microelectronics, data storage and food packaging industries. Technologies involving nano- or microfabricated polymeric structures such as micro total analysis systems (μ-TAS or "lab on a chip"), biomedical devices, polymer light-emitting diodes, molecular electronics and organic flat panel displays often require metallization to form integrated electrodes or sensors fabricated directly onto the polymeric substrate. These technologies typically are formed from vapor deposited metal films less than 200 nm in thickness.

A. K. Mo, V. L. Brown, B. K. Rugg, Prof. T. C. DeVore, Dr. X. F. Hu, Prof. W. C. Hughes, Prof. B. H. Augustine
Center for Materials Science
MSC 4310, James Madison University
Harrisonburg, VA 22807, USA
E-mail: augustbh@jmu.edu
Dr. H. M. Meyer
Microscopy Group
Oak Ridge National Laboratory
1 Bethel Valley Road, P.O. Box 2008, Oak Ridge, TN 37813, USA

DOI: 10.1002/adfm.201201955

The interface between metal thin films and polymeric substrates has been the subject of study for several decades.[1] Metals deposited from the vapor phase generally exhibit relatively poor adhesion to polymeric substrates since the cohesive forces acting between metals atoms can be up to two orders of magnitude stronger than the adhesive forces acting between the adsorbed metal atom and the polymer leading to the metal atoms bonding with one another rather than forming an adhesive bond with the substrate.[2] This is particularly evident for the deposition of noble metals such as Cu, Ag, Au, or Pt that do not form strongly bonded oxides resulting in a worst-case scenario for deposition onto many common polymeric substrate materials.[3]

Process engineers have developed Au and Pt interconnects and electrodes in silicon-based microelectronics and microelectromechanical systems (MEMS) by using a metal adhesion layer. Typically, this is produced by vapor deposition of a <5-nm layer of reactive metal such as Cr or Ti, that can form a chemical bond with polar atoms on the surface.[4] The Au or Pt film is then deposited without breaking vacuum so that the surface atoms on the adhesion layer do not oxidize prior to deposition of the noble metal thin film. The resulting two layer structure produces a metal film that is conformal and well-bonded to the Si, SiO_2, or other inorganic substrate.

Several groups have reported successful deposition of Au thin films onto a variety of polymeric substrates through surface pretreatments such as O_2,[5,6] O_2/CF_4,[2] or Ar[7,8] plasma exposure, irradiation with ultraviolet laser light[9] or ion beams.[10] Two primary mechanisms have been reported for the improved adhesion of noble metals related to changes in the surface roughness and surface chemistry.[11] Increased surface roughness provides more surface area at the metal/polymer interface. Surface chemical modification strategies generally involve adding more polar bonds to the surface. Many of the gains made by plasma modification of the surface are short-lived and have limited effectiveness in improving Au/polymer adhesion.

Recently, we reported improved adhesion of magnetron sputter deposited Cr/Au films onto poly(methyl methacrylate) (PMMA) substrates by over a factor of four compared to cleaned

substrates by spin-casting chlorinated solvents onto the PMMA surface prior to metal deposition.[12] To briefly summarize those results, samples that had been pretreated with chloroform ($CHCl_3$) improved from less than 20% adhesion of a 121 dot array of 1.5-mm diameter Cr/Au dots onto PMMA samples to nearly 90% adhesion, while samples treated with nonpolar solvents such as hexane had no appreciable gain in adhesion. PMMA pretreated with a remote O_2 plasma exhibited less than 30% adhesion. Samples in which $CHCl_3$ was spin-cast on the surface and degassed in a vacuum environment below 5×10^{-6} Torr for 96 h showed nearly the same adhesion as the as-deposited $CHCl_3$ samples while the adhesion of toluene ($C_6H_5CH_3$)-treated samples degassed under vacuum returned to the same level as the as-cleaned control sample (≈20% adhesion).[12]

In the prior study, two possible mechanisms for the improved adhesion were proposed. One hypothesis was that the solvent preferentially oriented the ester groups in the PMMA chain towards the surface producing a more polar oxygen-rich surface that bonded to the Cr atoms. The second was that residual solvent molecules present on the PMMA surface interacted with the sputter-deposited Cr atoms. Spectroscopic evidence lending support for the second mechanism was provided by attenuated total reflection Fourier transform infrared spectroscopy (ATR-FTIR) in which the C–Cl E stretching band of $CHCl_3$ was observed up to 7 days after solvent deposition. However, the ATR-FTIR data did not conclusively establish that the residual solvent resulted in the enhanced metal adhesion.[12]

In the present study, we report that thin films of Au or Pt deposited directly onto PMMA without an adhesion layer also exhibit an adhesion improvement when the PMMA is pretreated with a variety of halogenated solvents. We have broadened the study to include electron-beam (e-beam) evaporation in addition to magnetron sputter deposition and demonstrate that vapor-exposed solvent pretreatments can be nearly as effective as spin-cast samples. Finally, we have performed density functional theory (DFT) calculations on a model polymer/solvent/metal system to better understand the mechanism for the improved metal adhesion during the initial nucleation stage of the metal deposition. Comparison of the results of the calculations to high resolution X-ray photoelectron (XPS) and FTIR spectroscopic data obtained for the metal films provide support for the model presented to explain the enhanced adhesion. Similar spectroscopic and DFT studies have been reported in the last decade by the Allara group on alkanthiol self-assembled monolayer (SAM) terminated Au substrates to model the interaction of metal thin films deposited onto organic surfaces in which the surface chemistry can be modulated by controlling the terminal group of the SAM.[13–17]

2. Results

The percentage of Au and Pt remaining for samples deposited via e-beam evaporation after the tape test for the halogenated solvent pretreatments, the IPA cleaned samples, and remote O_2 plasma treated samples are shown in **Figure 1**. The inset of Figure 1 shows the adhesion of Au on PMMA as the exposure time to the $CHCl_3$ vapor increased. The adhesion obtained after 300 s of vapor-exposure is similar to the adhesion obtained

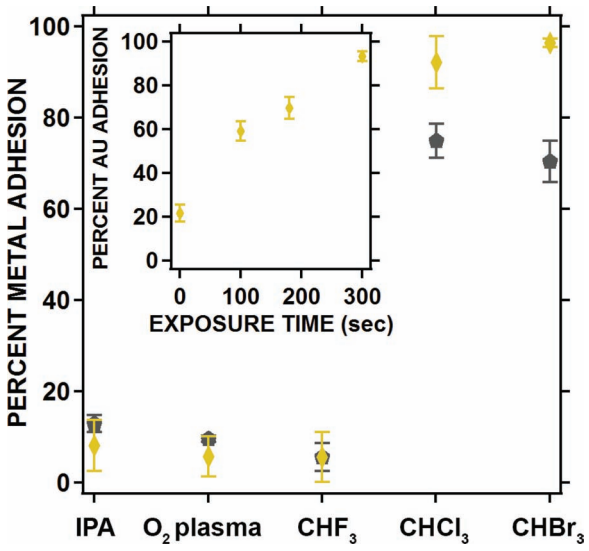

Figure 1. Tape test adhesion results for 100-nm-thick e-beam evaporated Au (gold diamonds) and Pt (grey pentagons) thin films with the following pretreatment conditions: isopropyl alcohol (IPA) sonicated for 10 min, then dried with N_2; remote O_2 plasma (25 W, 500 s, 5% O_2: 95% N_2); gas-phase CHF_3, spin-cast $CHCl_3$ and spin-cast $CHBr_3$ at 1000 rpm for 45 s and 300 rpm for 15 s. Inset is the effect of vapor-exposed $CHCl_3$ maintained at 2000 Torr. Error bars are one standard deviation of the mean. ($N \geq 15$).

for spin-cast samples. This suggests that the chemistry of the solvent-polymer interaction is critical, and the adhesion improvement is not due to an effect related to fluid dynamics, spin-casting, or the dissolution and resolidification of the polymer caused by the liquid solvent interacting with the solid polymer surface. Recent work has shown that vapor phase $CHCl_3$ can be used to polish PMMA microdevices.[22] Further adhesion data is shown in the supporting material including comparing Au thin film adhesion for films produced using e-beam and magnetron sputter deposition (Figure S1, Supporting Information), and for samples degassed under vacuum at $<5 \times 10^{-6}$ Torr for 96 h prior to deposition using e-beam evaporation (Figure S2, Supporting Information). As shown in these figures, there are no appreciable differences in adhesion for either deposition method or length of time after solvent pretreatment. As was previously reported,[12] the failure of the vacuum degassing to change the adhesion (Figure S2, Supporting Information) suggests that the solvent must have a relatively strong interaction with the PMMA which will be discussed further.

In order to better understand the results shown in Figure 1, and Figure S1 and Figure S2 in the Supporting Information, EGA-FTIR was performed on spin-cast $CHCl_3$ and vapor-exposed CHF_3 samples. The $CHCl_3$ samples were stored for nine days after deposition, and the CHF_3 samples were stored for five days after vapor exposure and then analyzed. Both were stored in a N_2 dry box at 23 °C and atmospheric pressure. **Figure 2** shows a waterfall plot of the EGA-FTIR spectra taken over a temperature range from 50–150 °C for $CHCl_3$. The analogous plot from 90–146 °C for CHF_3 is shown in Figure S3 (Supporting Information). Using these data, a van't Hoff plot for the desorption of the halogenated solvents from the bulk

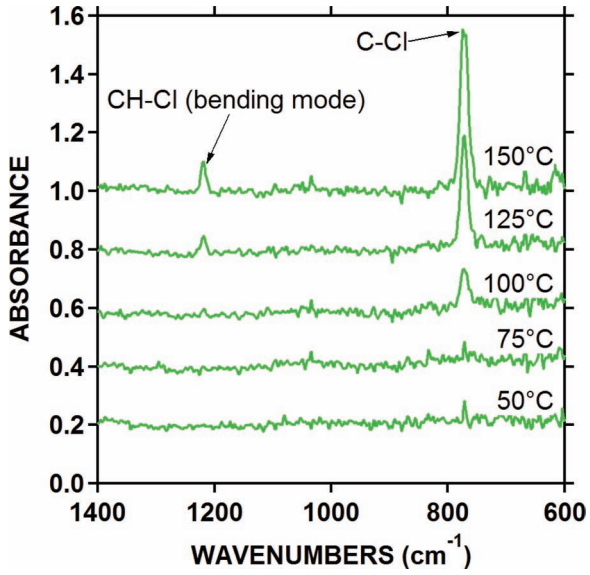

Figure 2. Waterfall plot of EGA-FTIR of $CHCl_3$ exposed PMMA. Samples were spin-cast, stored in a N_2 dry box at 23 °C for 9 days, then heated from 50–150 °C.

PMMA was prepared by taking the natural log of the integrated peak intensity of the primary IR absorption peak (750 cm^{-1} for the C–Cl and 1151 cm^{-1} for the C–F stretching modes in $CHCl_3$ and CHF_3, respectively) and plotting against 1/T and is shown in **Figure 3**. The slope of Figure 3 is directly proportional to the enthalpy of solvent desorption (ΔH_{des}) from the bulk PMMA with $CHCl_3$ giving 36.2 kJ mol^{-1} and CHF_3 producing 63.8 kJ mol^{-1}. EGA-FTIR was attempted for $CHBr_3$ exposed surfaces, however

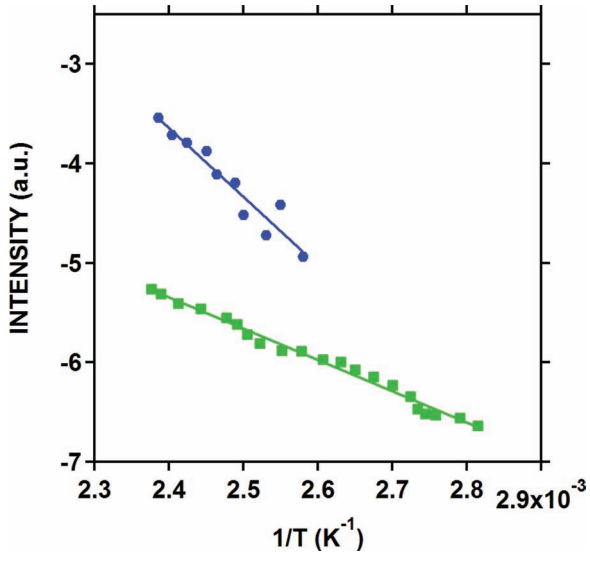

Figure 3. van't Hoff plot of ln(integrated FTIR peak area) vs T^{-1} for $CHCl_3$ (green) and CHF_3 (blue). $CHCl_3$ sample was spin-cast, stored 9 days in a N_2 dry box at 23 °C. The CHF_3 sample was vapor exposed for 24 h at 2000 Torr and stored 5 days in N_2 dry box at 23 °C. $\Delta H_{des(CHCl3)}$ = 36.2 kJ mol^{-1} and $\Delta H_{des(CHF3)}$ = 63.8 kJ mol^{-1}, determined from slope.

the C–Br stretching peak and ambient CO_2 peaks are strongly blended making it difficult to quantitatively monitor the C–Br desorption peak.

Figure 4, **Figure 5**, and Figure S4 show normalized high resolution core-level XPS data for several analysis regions and sample types. Vertical dashed lines on these figures indicate the peak energies reported in the literature for the major chemical bonding states in each region. These figures have been color-coded. The data from samples pretreated with CHF_3 are in blue, $CHCl_3$ are in green and $CHBr_3$ are in red. Figure 4 shows the halogen binding energy region (F 1s, Cl 2p and Br 3p) for solvent-exposed PMMA prior to and following e-beam evaporation of ≈30 Å of Au and of Pt. The 30-Å metal films were required to observe the emitted photoelectrons from the metal/PMMA interface. In Figure 4, the F 1s peak at 684.6 eV is a singlet, while the Cl 2p and Br 3p peaks are doublets due to spin-orbit coupling. Figure 5 shows the O 1s region grouped as follows: untreated PMMA and PMMA with solvents only labeled "PMMA", PMMA with 30 Å of e-beam evaporated Au or Pt without solvent and with solvent pretreatment labeled "PMMA/Au" or "PMMA/Pt", respectively. The doublet observed for the as-cleaned PMMA control is consistent with the two types of O bonding present in PMMA. The low binding energy peak at a binding energy of 531.99 eV (49.5%) has been assigned to C=O, and the higher binding energy peak at 533.77 eV (50.5%) is assigned to the bridging O in the ester bond (–O–).[23] The 50:50 peak area ratio is expected in an untreated PMMA sample as the only O present in PMMA is the 1:1 stoichiometric ratio of the two types of O atoms in the ester functional group. Figure S4 (Supporting Information) shows the Au and Pt 4f regions for 30 Å of metal deposited directly onto PMMA (no solvent pretreatment) and solvent-exposed PMMA followed by Au or Pt deposition. The characteristic doublet is again due to spin-orbit coupling of the $4f_{7/2}$ and the $4f_{5/2}$ orbitals. Table S1–S3 in the Supporting Information show the peak identification, binding energy, and peak fitting data for the spectra in Figure 4,5, and Figure S4, respectively.

Additional XPS data (Figure S5 in the Supporting Information) shows the time evolution of the relative peak area of the Cl $2p_{3/2}$ peak for a $CHCl_3$-PMMA sample after spin-casting. This data was generated by focusing the X-ray to a 400 μm spot and analyzing only the Cl $2p_{3/2}$ region at approximately 0.33 min per pixel. The sample stage was then translated by 1.5 mm and the process was stepwise repeated overnight producing an 11 × 10 pixel intensity map of integrated pixels. The map of the integrated Cl $2p_{3/2}$ peak intensity is shown in the inset to Figure S5. The Cl $2p_{3/2}$ peak area along the diagonal of the inset (indicated with the black line) is plotted in Figure S5. There is an initial significant drop in Cl $2p_{3/2}$ peak intensity as the bulk solvent evaporates from the surface, but there is a measurable Cl peak over 5 h after solvent deposition even though the sample was maintained in a ≈10^{-10} Torr ultrahigh vacuum environment. The Cl $2p_{3/2}$ peak must be due to residual solvent that does not readily desorb after deposition. The spectroscopic evidence of residual solvent is consistent with the ATR-FTIR data of our previous study[12] and the EGA-FTIR results shown in Figures 2,3 and Figure S3 (Supporting Information). We have not performed a similar time-evolution XPS study on either the $CHBr_3$ or CHF_3 samples.

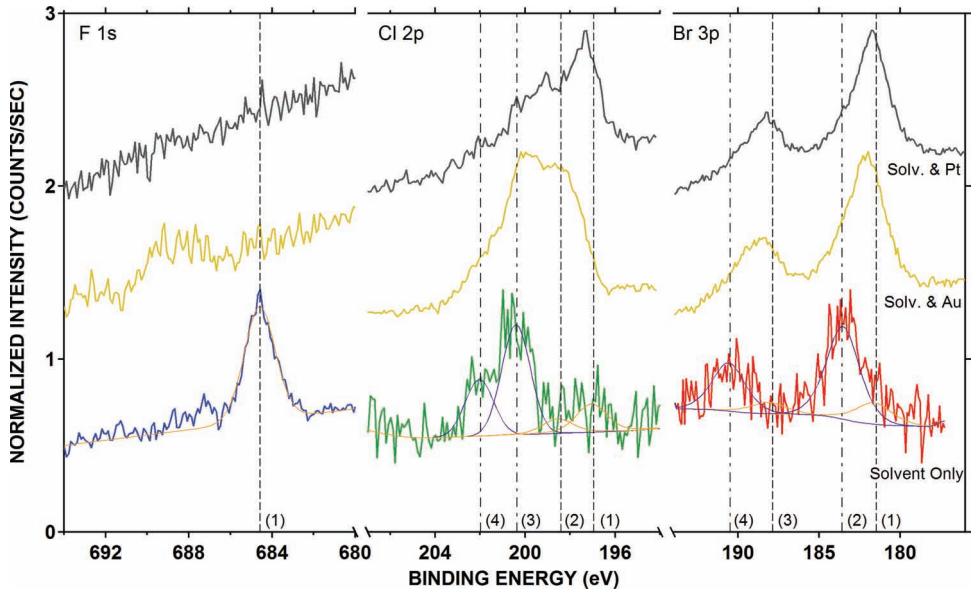

Figure 4. Normalized high-resolution XPS data of halogen binding energy region for CHF_3 (blue), $CHCl_3$ (green) and $CHBr_3$ (red) exposed PMMA. Solvent treatment conditions were as in Figure 1. 30 Å of Au (gold) and Pt (grey) were deposited by e-beam evaporation. $CHCl_3$ and $CHBr_3$ were analyzed 2–3 days after spin-casting, CHF_3 was analyzed immediately after removal from exposure chamber. Vertical dashed lines indicate literature values for major chemical binding energy states for the F 1s, Cl 2p and Br 3p regions. Spin orbit coupling peaks ($np_{3/2}$ and $np_{1/2}$) resulting from the same chemical species are indicated with the same type of vertical line.

3. Discussion

In our prior report, two possible mechanisms were proposed: (1) polar solvents were producing a surface in which polar ester groups in PMMA had been preferentially aligned to produce a favorable interaction between the Cr adhesion metal and the surface O atoms, and (2) the presence of residual solvent molecules resulted in an interaction between sputter deposited Cr atoms and the surface solvent molecules.[12] In the prior study, ATR-FTIR data showed a broad IR absorption peak between 755–765 cm^{-1}. This was assigned to bending modes in the PMMA at 750 cm^{-1} and the C–Cl E stretching band between 755–765 cm^{-1}. The time-evolved data over 7 days suggested that there were actually two peaks that could be attributed to C–Cl bonding. The primary peak at 751 cm^{-1} is characteristic of bulk $CHCl_3$. There was also a smaller shoulder at 761 cm^{-1} that was first observed 38 h after deposition and became much more pronounced 7 days after deposition. We speculated this peak was due to an interaction between $CHCl_3$ and the PMMA which could be observed after the bulk solvent evaporated from the sample. Since the peak assignment of the 761 cm^{-1} peak was tentative and there was no definitive data to suggest that this residual solvent was responsible for the enhanced adhesion, additional data were required to establish the reason for the enhanced adhesion.

There is now ample analytical evidence from several complimentary techniques that halogen bonding is present in pretreated PMMA samples for several days after deposition. The aforementioned ATR-FTIR data suggested this,[12] and Figure 2–4, and Figure S3 and S5 (Supporting Information) provide compelling evidence that both Cl and Br are present in measurable quantities both at the surface and in the bulk.

Understanding the actual mechanism of the improved Au and Pt adhesion on PMMA substrates requires an understanding of the surface chemical bonding states present. This is done by using high resolution XPS to investigate the halogen regions in the three hydrohalocarbon samples in Figure 4 and Table 1 (Supporting Information). There is a significant difference between the metallized samples containing F compared to those containing either Cl or Br. The CHF_3 samples show evidence of F present in the spectra labeled "Solvent Only" with a single peak at 684.6 eV, but no evidence of F bonding after either Au or Pt is deposited. In contrast, there is a significant peak shift to a lower binding energy after metallization for both the $CHCl_3$ and the $CHBr_3$ samples. Four peaks have been used to fit the XPS data for the Cl 2p and the Br 3p regions shown in Figure 4. Looking at the "Solvent Only" samples for Cl, there is a higher binding energy doublet due to Cl $2p_{3/2}$ and Cl $2p_{1/2}$ electrons at 200.41 and 202.02 eV indicated with a dash-dot vertical line. The corresponding peaks for the Br $3p_{3/2}$ and $3p_{1/2}$ electrons are evident at 183.54 and 190.58 eV, respectively. These peaks are consistent with C–Cl or C–Br bonding. For example, the XPS spectrum of polyvinylidene chloride has a Cl $2p_{3/2}$ peak at 200.78 eV.[23] In the metallized samples, the low binding energy Cl $2p_{3/2}$ and $2p_{1/2}$ doublets at ≈198 and 199 eV indicated with a dashed vertical line are characteristic of a Cl atom bonded to a metal and are in agreement with the binding energy range for the Cl $2p_{3/2}$ peaks for Au–Cl and Pt–Cl bonding.[24,25] The low binding energy doublet in the metallized Br 3p spectra are seen at ≈182 and 189 eV for the Br $3p_{3/2}$ and $3p_{1/2}$ electrons, respectively. Thus, the data presented in Figure 4 clearly shows the presence of Au–X and Pt–X bonds where X is a halogen atom for both Cl and Br treated-surfaces but not for F treated surfaces. It should be noted that XPS for

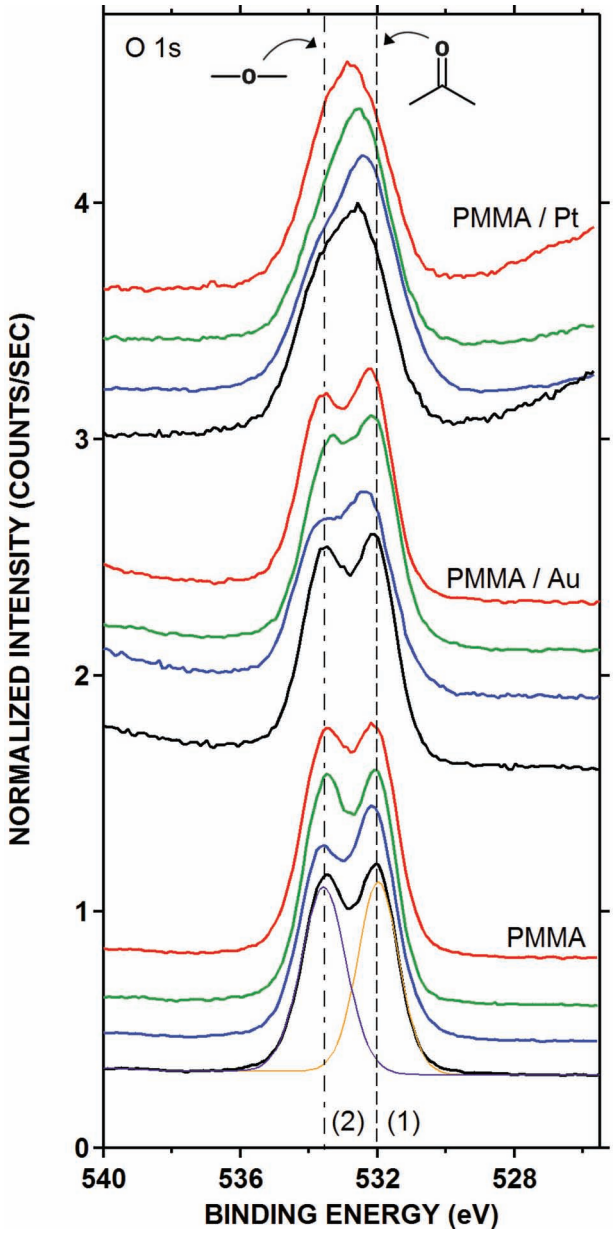

Figure 5. Normalized high-resolution XPS of O 1s binding energy region of PMMA exposed to CHF_3 (blue), $CHCl_3$ (green) and $CHBr_3$ (red) under the same solvent exposure conditions as Figure 4. Spectra labeled "PMMA" are PMMA only (black) and solvent-exposed prior to metal deposition. Spectra labeled "PMMA/ Au" are 30 Å of Au e-beam evaporated directly onto PMMA (black) and solvent-exposed prior to Au deposition. Spectra labeled "PMMA/ Pt" are 30 Å of Pt e-beam evaporated directly onto PMMA (black) and solvent-exposed prior to Pt deposition.

both the $CHCl_3$ and $CHBr_3$ "Solvent Only" samples were measured 2–3 days after spin-coating/packaging/shipping to Oak Ridge, TN/loading into the XPS analysis chamber, while the F data was obtained within minutes after venting the CHF_3 exposure chamber and loading the samples directly into the XPS load-lock. Samples that were CHF_3 treated and shipped for XPS analysis did not show any evidence of F under any conditions suggesting that the CHF_3 molecules readily desorb from the PMMA surface.

Results of high-resolution XPS data for the O 1s region shown in Figure 5 and Table 2 give evidence of the likely bonding mechanism for metals onto the $CHCl_3$ and $CHBr_3$ treated surfaces. As mentioned, there are two characteristic peaks known for PMMA. The low binding energy peak at a binding energy of 532.21 eV has been assigned to C=O, and the higher binding energy peak at 533.77 eV is due to the bridging O in the ester bond (–O–).[23] Subtle changes in both the peak shape and intensity ratio occur depending on the type of surface treatment performed with the most significant changes occurring in the Pt coated samples seen in Figure 5.

The higher binding energy of the bridging O in PMMA indicates that it is the more electronegative of the two oxygen atoms, and thus would be most likely to interact with an electropositive molecule. While there is relatively little difference in the $CHCl_3$ and the $CHBr_3$ solvent-only treated samples compared to the PMMA sample, the CHF_3 treated sample shows nearly a 10% decrease in the bridging O peak area relative to the C=O peak. This is most likely due to the CHF_3 acting as a Lewis acid and enabling an ester hydrolysis reaction. Thus when PMMA is exposed to high pressures of CHF_3 gas for an extended time, it is likely that the surface ester bonds are being broken in the presence of water producing a carboxylic acid-terminated surface. This reduces the concentration of bridging O present at the surface reducing the area of this peak relative to the C=O peak. This same phenomena is not observed in the $CHCl_3$ or $CHBr_3$ because the CHF_3 is a much stronger Lewis acid due to the higher electronegativity of the F atoms compared to Cl or Br.

There are changes observed in the O 1s peaks for both the Au and Pt coated surfaces with the most significant occurring in the bridging O peak for both metals. Specifically, the bridging O peak intensity drops either subtly in the case of Au coating, or significantly in the case of Pt coating. The CHF_3 treated surfaces for both metals result in the largest drop in –O– peak intensity presumably due to the aforementioned chemical reaction between CHF_3 and the bridging ester O. The Au coated surfaces show a 5% reduction in relative peak area in the bridging O peak compared to the uncoated control, and no change compared to the Au coated sample without any solvent pretreatment. The Pt coated samples show a 20% change in relative peak area in the bridging O compared to the PMMA control, and a 15% decrease compared to the Pt coated sample without any solvent pretreatment. There is also an increase in the average peak area full width at half maximum (FWHM) in the peaks assigned from the control and the solvent-only coated samples (≈1.5 eV), to the Au coated (≈1.6 eV) and the Pt coated (≈2.0 eV). This peak broadening is indicative of a distribution of bonding states that cannot be resolved by the XPS instrument. The peak shape and the changes in FWHM suggest that the local bonding environment of the bridging O is shifting to a lower binding energy. This is particularly evident in the Pt sample in which the doublet is no longer observed and the overall peak position is centered between the two peaks in PMMA. This broad peak is a combination of the contribution from each O bonding state at the sample surface from the PMMA and any changes that occurred from bonding with the

Pt. Bonding to a metal generally results in a peak shift to a lower binding energy. The fact that the bridging O peak has decreased so significantly and there is now an intermediate peak between the PMMA peaks suggests that the metal is bonded preferentially to the bridging O.

The high resolution 4f metal regions for Au and Pt are shown in Figure S4 and Table 3 in the Supporting Information. Samples treated with CHF_3 show no change to the 4f peak in either the Au or the Pt, while the $CHCl_3$ and $CHBr_3$ exhibit a slight shift to a higher binding energy compared to the untreated sample or the CHF_3 sample. While the slight shift to higher binding energy is too small to draw meaningful conclusions, a higher binding energy for the metal bonded to a more electronegative halogen atom is consistent with the expected change in the XPS trends.

This experimental data is best understood by considering the non-complexing behavior of $CHCl_3$ or $CHBr_3$ with PMMA.[26] "Complexing" and "non-complexing" are terms used in the polymer literature to describe the interaction between a solvent and the polymer chains in solution to indicate the formation of a Lewis acid-base adduct between the solvent and the polymer chain. More specifically, the terms "complexing" and "non-complexing" refer to chain-chain interactions and not the interaction between the solvent and polymer. A complexing solvent means that there is little or no Lewis acid-base interaction between the solvent and the polymer chain so the polymer chains are able to form a complex in solution. In the case of PMMA, the polar ester groups would generate chain-to-chain dipole interactions producing a polymer complex in solution.[27] In a solvent categorized as non-complexing, the solvent and polymer interact strongly through the formation of a Lewis acid-base adduct which effectively screens the dipole charge and minimizes interactions between chains. Specifically in the case of halogenated alkanes in the form, $H–CX_y$, where X is the halogen atom, the adduct is formed between the H on the solvent molecule acting as a Lewis acid and the O atoms in the ester group in PMMA acting as a Lewis base. This interaction has recently been reported to direct self-assembly to form a supramolecular complex in a polymer-azobenzene complex through halogen bonding.[28] An empirical parameter called the Gutmann acceptor number has been used to quantify the degree of Lewis acid-base interaction (i.e., complexing power).[29–32] Lower Gutmann acceptor numbers are assigned to complexing solvents and higher acceptor numbers are assigned to non-complexing solvents. The correlation between Gutmann's acceptor number and Au thin film adhesion will be discussed below.

In order to better understand a molecular level cause for the enhanced metal adhesion in the initial stages of nucleation, we have performed DFT calculations on a simplified model consisting of a MDP molecule to represent the PMMA monomer, a solvent molecule, and a metal atom. Each molecule was geometrically optimized by minimizing the energy. These molecules were then allowed to interact starting from several different configurations by minimizing the energy of the system. Typical results are shown in **Figure 6**. If the methyl groups were oriented opposite the C=O group in MDP to minimize steric hindrance, the most energetically favored configuration between the solvent molecule and the MDP was that in which the solvent molecule formed a Lewis acid-base adduct between

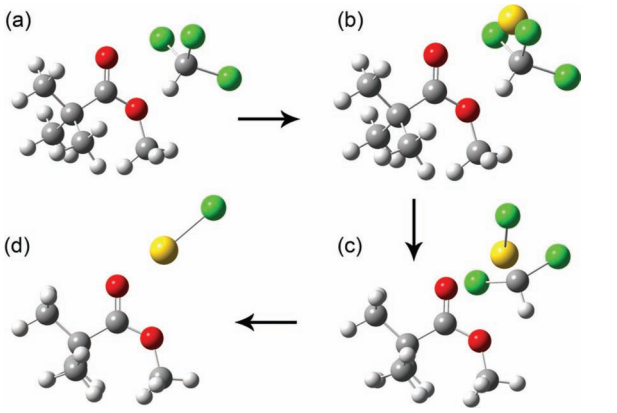

Figure 6. Model of metal-solvent-polymer interaction as determined by density functional theory calculation using methyl 2,2-dimethylpropanoate as a model system for PMMA. a) polymer interaction with $CHCl_3$, b) introduction of Au atom into polymer-$CHCl_3$ Lewis acid-base adduct, c Au insertion into C–Cl bond of $CHCl_3$, and d) O–M–Cl adsorbate remaining.

the H on the halogenated solvent molecule in the form $H–CX_3$ aligned toward the O atoms in the ester group forming an analogous configuration to a hydrogen bond as shown in Figure 6a. Calculated energies generated from molecular modeling for this interaction were on the order of 35–42 kJ mol^{-1} consistent both with the energies of a Lewis acid-base adduct and with experimentally derived ΔH_{des} of 36.2 kJ mol^{-1} for $CHCl_3$ calculated from the van't Hoff plot in Figure 3. After the solvent-monomer calculation had minimized (Figure 6a), a Cu, Cr, or Au atom was introduced into the pocket produced by the O atoms in the MDP and the X atom from the solvent and the equilibrium structure was determined by minimizing the energy of the system. No restrictions were used for these calculations and the chemical bonds between atoms could be changed if it produced a lower energy structure. For many different starting configurations, these calculations predicted that a lower energy complex was formed when the metal atom inserts itself into the X–C bond as shown in Figure 6b. It required little energy for the remainder of the solvent ($HCCl_2$ or $HCBr_2$) to desorb (presumably after forming a new C–C bond which was not modeled) (Figure 6c) leaving behind a Lewis acid-base interaction of O–M–X as shown in Figure 6d where M is the metal atom.

Prior work on alkanethiol SAM systems on Au substrates has shown that certain terminal groups and metals result in a similar insertion reaction.[13–16,33,34] SAMs have been used as a model system to study the metal/organic interface during the initial stages of metal film nucleation since highly ordered SAM structures can be created on a Au substrate, and the terminal group on the alkanethiol can be changed to significantly modify and control the surface chemistry ranging from hydrophobic to hydrophilic and acidic to basic. DFT modeling of a simple alkanethiol/metal system in conjunction with surface spectroscopy (XPS, ISS, ToF-SIMS) has been used to show that Al atoms deposited onto a $–CO_2CH_3$ and –COOH terminated SAM resulted in a –O–Al–H surface where the Al inserted itself into the C=O bond,[14] while Walker showed that with Cu deposited onto the same surface, the metal did not insert itself

into the ester bond, but did form a complex with the surface.[16] The results of these studies suggest that the actual surface chemistry of the initial nucleation stages of metal film growth on an organic surface depends critically on the specific metal and the surface functional groups present.

The result shown in Figure 6a indicates that the solvent molecules interact more strongly with the bridging ester O compared to the C=O if steric effects are minimized. This is consistent with the XPS data for the O 1s peak previously discussed in regard to Figure 5. The interaction of the newly formed metal halide with the oxygen atom would produce a change in the local bonding environment in the bridging O atom which is consistent with prior XPS data for Ni films deposited onto PMMA[35] and with a Cu film vapor deposited onto an ester terminated alkanethiol ($HS–(CH)_{15}–CO_2CH_3$.[16] The higher binding energy of the bridging O in PMMA indicates that it is more electronegative and this would be more likely interact with the positive dipole of the polar solvent molecules as suggested by the DFT calculations.

The resulting O–M–X bonding configuration at the surface would be stabilized since the electron density is expected to move from the metal atom to the electronegative halogen atom. Since the partial positive charge on the metal atom will interact more strongly with the electron-rich oxygen atoms, a stronger M–O interaction is expected that will result in enhanced stability of the M–O interaction. The subsequent arrival of a metal atom during the deposition process would see halogen atoms bonded to metal atoms on the surface and would form an energetically favorable M–X cluster on this surface. This is also consistent with the M–X Cl 2p and Br 3p bonding peaks evident in the high resolution XPS data shown in Figure 4.

Although the actual energies calculated using DFT are not expected to give experimental accuracy at this level of approximation, the results of the DFT modeling are consistent with the reported experimental data. The molecular modeling supports the presence of residual solvent molecules interacting with the PMMA having an interaction energy of a hydrogen bond consistent with the EGA-FTIR spectroscopic data (Figure 2,3 and Figure S3 in the Supporting Information) and with the known Lewis acid-base adduct formation in non-complexing solvents with PMMA.[36] Moreover, the preferred interaction between the metal atom and the bridging O is consistent with the suppression of the high binding energy O 1s peak in the XPS data shown in Figure 5.

In Figure 1 and Figure S1 (Supporting Information), both Au and Pt adhesion were significantly enhanced using either $CHBr_3$ or $CHCl_3$, but not with CHF_3. In Figure 4, XPS spectroscopy clearly shows the presence of C–Cl and C–Br bonding on the surface after either vapor or liquid halogenated solvent exposure, but not C–F bonding. The effectiveness of each solvent can be understood in light of the bonding enthalpies of the various chemical reactions.

The DFT calculation for the model system of the initial metal nucleation indicates that there are three major bonding steps in the adhesion of the metal on the surface that need to be considered. These are (1) the solvent-polymer adsorption interaction (Figure 6a), (2) the metal-solvent insertion reaction (Figure 6b), and (3) the metal-polymer adsorption reaction (Figure 6d). These three reactions can be represented by the following three thermodynamic equations:

$$\mathrm{H-CH_yX_z + Polymer \rightarrow Polymer\cdots H-CH_yX_z} \quad (1)$$

$$\mathrm{M + X-CH_yX_z \rightarrow M-X + CH_yX_z} \quad (2)$$

$$\mathrm{M-X + Polymer \rightarrow Polymer\cdots M-X} \quad (3)$$

With the combined assumption that the second reaction is the most important in the production of enhanced stability and that it is a vapor phase process, the difference in the bond energies between the $X–CH_yX_z$ and the M–X bonds can be used to estimate the effectiveness of the process. If the entropy, ΔS, for Reaction (2) is assumed to be small, the Gibb's free energy, ΔG, is approximately equal to ΔH_{rxn}. If the small contributions caused by the translational and internal energy of the reactant and product molecules are also assumed to be zero, the difference between the bond dissociation energies ($D°$) of the M–X and $X–CH_yX_z$ bonds relate to ΔG as:[37,38]

$$\Delta G \approx \left[D^\circ(\mathrm{M-X})\right] - \left[D^\circ(\mathrm{X-CH_yX_z})\right] \quad (4)$$

The exact $X–CH_yX_z$ energy depends on the compound and the bond being broken. The $Cl–CHCl_2$ molecule has a literature gas phase bond dissociation energy of 311 kJ mol^{-1}.[39] This suggests that any metal with a M–Cl bond on the order of 311 kJ mol^{-1} should form the M–Cl bond from Reaction (2). It should be noted that the terms ignored in making this estimate could change the exact value needed to produce an exergonic process for Reaction (2) somewhat, but this is a reasonable approximation to the value needed. The literature values for the Au–X bonds are as follows: Au–F (294 kJ mol^{-1}), Au–Cl (280 kJ mol^{-1}), and Au–Br (213 kJ mol^{-1}).[39] The bond dissociation energies of $F–CHF_2$ and $Br–CHBr_2$ are 534 and 275 kJ mol^{-1}, respectively.[39] Thus, the increased bond strength of the $F–CHF_2$ bond explains why despite the fact that CHF_3 has a nearly two times larger ΔH_{des} compared to $CHCl_3$ as measured from the van't Hoff plot in Figure 3, there is no evidence of adhesion shown in Figure 1 and Figure S2 (Supporting Information) for CHF_3 compared to the control samples. This also explains why no M–F bonding is seen in the XPS in Figure 4. Equation (4) also suggests that since different hydrohalocarbons exhibit different chemical bond strengths, the adhesion of metals to the polymer surface can be tailored depending on the bond energies of the pretreatment molecule and the M–X bond being formed with CHF_3 acting as a negative control.

In order to better understand the types of solvents that can improve the adhesion of metals onto PMMA, we have performed Au thin film adhesion tests using a variety of solvents with a range of Gutmann acceptor numbers as shown in **Figure 7**. Solvents with a high Gutmann acceptor number (i.e., non-complexing solvents) result in significantly improved adhesion compared with complexing solvents. Investigations are ongoing to determine if this is a broadly applicable principle across many types of polymer/metal interactions, or whether this is specific to PMMA and Au or Pt films.

4. Conclusions

We report significantly improved adhesion of Au and Pt thin films onto PMMA substrates compared to either IPA cleaned or

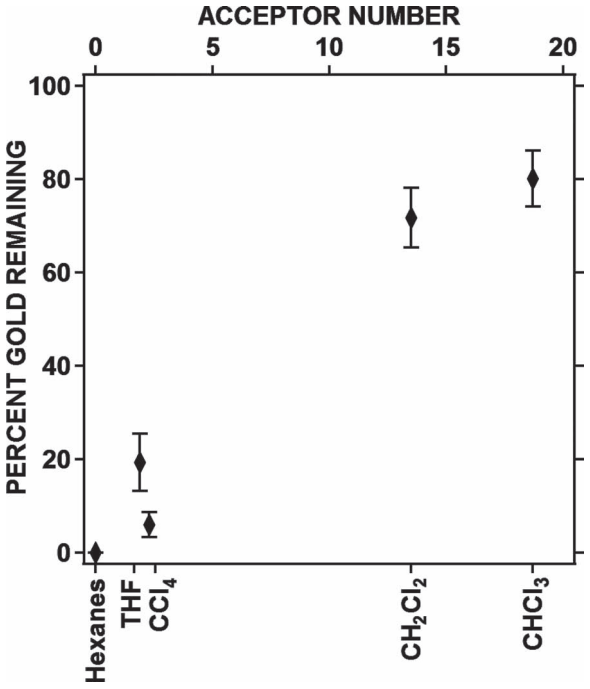

Figure 7. Percentage of Au remaining as a function of Gutmann acceptor number for a variety of complexing and non-complexing solvents.

remote O_2 plasma-treated substrates by exposing the PMMA to either spin-cast or vapor-exposed halogenated organic solvents with and without the use of a metal adhesion layer. Spectroscopic evidence indicates the improvement of noble metal thin film adhesion is caused by residual halogenated solvent molecules that have formed a stable Lewis acid-base adduct with the PMMA. Non-complexing solvents with a high Gutmann acceptor number such as $CHCl_3$ and $CHBr_3$ form a Lewis acid-base adduct with the PMMA by interacting with the ester groups of the PMMA and remain on the surface long after the bulk solvent has evaporated. DFT calculations using a model system and XPS data suggest that this complex is formed through a Lewis acid-base adduct between the solvent molecule and the bridging O in the PMMA. The complexed solvent molecules then react with the metal atoms during the deposition process to produce a M–X bond that reacts at the surface. A four-fold enhancement in metal adhesion can be achieved with less than 5 min though solvent vapor exposure. No changes in surface morphology or roughness were observed indicating that the surface is left undamaged by this treatment. This vapor exposure technique is potentially attractive as a technology for enhancing the adhesion of metal films onto PMMA devices such as μ-TAS, polymer MEMS, photonic, or biomedical devices.

5. Experimental Details

Samples: PMMA substrates (2.54 cm × 2.54 cm) were cleaned by sonicating in isopropyl alcohol (IPA) and prepared as previously described.[12] The hydrohalocarbons, liquid-phase bromoform ($CHBr_3$) and chloroform ($CHCl_3$), and gas-phase fluoroform (CHF_3), were used as received (Sigma-Aldrich). Metallization was accomplished by e-beam evaporation for either Au or Pt films or by magnetron sputter deposition for Au films only. In either case, no adhesion layer was used and the resulting metal film thickness was nominally 100 nm for the adhesion study. Metal film thickness was monitored by a quartz crystal microbalance (QCM) and a calibration curve was developed over a range of deposition times and thicknesses. Samples prepared for the XPS study were nominally 30 Å in thickness to ensure that photoelectrons produced from the metal/PMMA interface could be detected. The metals used were 99.99% purity shot for the e-beam and a Au target (3″ × 1/8″) (≈7.6 cm x 0.32 cm) for the magnetron (Kurt J. Lesker Corp.). Two types of samples were prepared for each solvent pretreatment. One type of samples were obtained by metallization within 5 min after solvent exposure. The other type of samples were degassed in a 5×10^{-6} Torr vacuum for 96 h to allow time for the bulk solvent to desorb from the surface prior to metallization. spin-cast exposure to $CHCl_3$ and $CHBr_3$ was accomplished by deposition at 1000 rpm for 45 s followed by 300 rpm for 15 s as previously described.[12] Vapor-exposed samples of $CHCl_3$ and CHF_3 were also prepared. For the $CHCl_3$ samples, a chamber was designed consisting of a glass Petri dish (15-cm diameter) covered by a sheet of polydimethylsiloxane (PDMS) film (200-μm thick, Rogers Corp). $CHCl_3$ (100 mL) was placed in the Petri dish, and IPA cleaned PMMA chips were held by surface tension to the bottom side of the PDMS cover facing the solvent. The PDMS cover was sealed to the edge of the Petri dish and the samples were held in the chamber for times ranging from 0–10 min. Samples were then immediately loaded into the deposition chamber and metallized. A custom-built stainless steel reaction chamber was used to expose the samples to CHF_3. This chamber was flushed for 2 min with CHF_3 gas. The chamber was then pressurized with CHF_3 gas (2000 Torr) and the sample was exposed to it for times ranging from 0.5–24 h.

Material Characterization: Metal adhesion was determined by using a "tape test" measurement modified from the ASTM D3359–09 method; a semiquantitative method of determining adhesion of films onto substrates.[18] In the ASTM method, a series of cross-hatched cuts are made through a film and a 2.54 cm × 2.54 cm piece of tape is affixed to the surface and removed. In this study, an array of 121 metal dots was deposited through a shadow mask and the removal of the metal dots was recorded using a digital camera and a stereo optical microscope (Leica MZ6). The digital images were converted to grayscale and measured using digital image processing software as described previously.[12] A minimum of 15 trials of each surface type were prepared for adhesion testing. A Thermo Scientific K-Alpha XPS was used for surface analysis. Samples (1 cm × 1 cm) were mounted on a 6 cm × 6 cm sample holder and introduced in the analysis chamber through a turbo-pumped load-lock system. Base pressure in the analysis chamber was 6.0×10^{-10} Torr. A charge compensation system that consisted of low energy Ar ions and low energy electrons was used during XPS analysis to minimize charging effects since the PMMA samples are insulators. Pressure in the analysis chamber was 1.5×10^{-7} Torr during charge compensation. A monochromatic Al K-α X-ray source (1486.7 eV) was focused to a 400-μm diameter spot on the sample surface to generate photoelectrons. A double focusing hemispherical energy analyzer was used to direct photoelectrons emitted at 90° from the sample plane onto a 128-channel detector. Survey scans were acquired at 1 eV/step at a pass energy of 200 eV, while high-resolution core-level spectra were acquired at 0.1 eV/step and a pass energy of 50 eV. Data were acquired and analyzed using the Advantage Software package (v. 4.61). All spectra were charge corrected to 285.0 eV referencing the lowest binding energy C 1s peak of PMMA. Evolved gas analysis Fourier transform infrared spectroscopy (EGA-FTIR) was used to determine the chemical composition of evolved gases produced as solvent-treated non-metallized PMMA samples were heated from 50–150 °C. Details of the home-built EGA-FTIR apparatus have been described in detail previously.[19–21] Samples were prepared by etching a 1.5 mm × 1.5 mm grid array into the cleaned PMMA substrate using a CO_2 laser-cutter. The cuts were approximately 90% of the way through the PMMA substrate (≈700 μm in depth). Solvents were then spin-cast onto the uncut surface. Five cubic pieces (1.5 mm × 1.5 mm) were placed into a glass sample tube (9 mm O.D.) within 5 min after spin-casting. The tube was then attached to the stainless steel IR cell and evacuated to ≈1000 mTorr. The tube was then slowly heated using a resistively heated tube furnace as the IR spectrometer monitored the

IR spectra of the evolved gases. Since the amount of evolved gas was expected to be small, all of the evolved gas was collected in the IR cell. IR spectra were collected from 400–4000 cm^{-1} with 4 cm^{-1} resolution as the sample was heated. The evolved gas was identified by matching the observed IR frequencies to those tabulated in standard data bases and confirmed by comparing the spectrum of the evolved gas to standard spectra produced by vaporizing a few microliters of the hydrohalocarbon directly into the cell. A Veeco Dimension 3100 atomic force microscope (AFM) was used to measure the surface topography on representative samples in tapping mode using a standard Si probe (Bruker OTESPA probe, k ≈ 42 N m^{-1}, f ≈ 300 kHz). All imaged samples exhibited an average surface roughness (R_q) of between 2.5–4.0 nm with no discernible morphological feature changes that depended on the surface treatment suggesting that surface roughness and morphology do not play a role in the improved metal adhesion. Density functional theory (DFT- B3LYP with a 6-31G++ basis set for most calculations) modeling was performed using the Gaussian09 molecular modeling software on a 32-bit Windows PC. The PMMA substrate was modeled as the monomer (methyl 2,2-dimethlypropanoate [$(CH_3)_3CCO_2CH_3$] or MDP) in order to capture the chemistry of the organic backbone and the ester group while minimizing the computational requirements in the DFT calculation. This model was chosen to semi-quantitatively model the chemistry of the initial nucleation phenomena in a manner analogous to prior studies using Au-SAM organic/metal surfaces.[14–17] The geometries for MDP, CHF_3, $CHCl_3$ and $CHBr_3$ molecules were independently optimized by using DFT to minimize the energy as the geometry was changed. The geometries of the monomer complexed with solvent molecule were obtained by aligning the geometry optimized hydrohalocarbon of the solvent molecule with the ester group in the monomer and optimizing the structure with DFT. Several different starting positions for the solvents were considered including initially aligned with the CO and aligned with the bridging O in the ester group. Once the optimal geometry had been found for the monomer-solvent system, a metal atom was placed at various positions and optimized to find the lowest energy structure. Since DFT-B3LYP - 6-31G++ calculations could not be performed using Au, these calculations were performed using Cu ($^2S_{1/2}$) and most of the conclusions were based on these model calculations. Other first row transition metals such as Cr ($^6S_{5/2}$) were also performed to determine if these calculations would explain the increased adhesion observed previously.[12] Calculations with the Au atom were performed using DFT PBEPBE with a SDD basis set.

Supporting Information

Supporting Information is available from the Wiley Online Library or from the author.

Acknowledgements

The authors would like to acknowledge funding through the Polymers Program at the Division of Materials Research at the National Science Foundation, NSF-RUI Grant No. DMR-1005641, the Department of Defense ASSURE/NSF-REU program, Grant No. DMR-0851367 and the Oak Ridge National Laboratory's SHaRE User Facility, which is sponsored by the Scientific User Facilities Division, Office of Science, U.S. Department of Energy.

Received: July 13, 2012
Revised: September 27, 2012
Published online: October 18, 2012

[1] *Metallized Plastics: Fundamentals and Applications* (Ed: K. L. Mittal), Marcel Dekker, New York **1998**.
[2] W. T. Li, R. B. Charters, B. Luther-Davies, L. Mar, *Appl. Surf. Sci.* **2004**, *233*, 227.
[3] V. Zaporojtchenko, T. Strunskus, K. Behnke, C. Von Bechtolsheim, M. Kiene, F. Faupel, *J. Adhes. Sci. Technol.* **2000**, *14*, 467.
[4] J. C. Hoogvliet, W. P. V. Bennekom, *Electrochim. Acta* **2001**, *47*, 599.
[5] J. M. Grace, L. J. Gerenser, *J. Dispers. Sci. Technol.* **2003**, *24*, 305.
[6] M. Collaud, P. Groening, S. Nowak, L. Schlapbach, *J. Adhes. Sci. Technol.* **1994**, *8*, 1115.
[7] V. Svorcik, V. Kotal, P. Slepicka, O. Blahova, P. Sutta, V. Hnatowicz, *Polym. Eng. Sci.* **2006**, *46*, 1326.
[8] V. Kotal, V. Svorcik, P. Slepicka, P. Sajdl, O. Blahova, P. Sutta, V. Hnatowicz, *Plasma Process. Polym.* **2007**, *4*, 69.
[9] S. Petit, P. Laurens, J. Amouroux, F. Arefi-Khonsari, *Appl. Surf. Sci.* **2000**, *168*, 300.
[10] A. M. Ektessabi, K. Uamaguchi, *Thin Solid Films* **2000**, *377*, 793.
[11] A. Thran, M. Kiene, V. Zaporojtchenko, F. Faupel, *Phys. Rev. Lett.* **1999**, *82*, 1903.
[12] A. K. Mo, T. C. DeVore, W. C. Hughes, V. P. Zungu, L. L. Lee, B. H. Augustine, *J. Vac. Sci. Technol., A* **2011**, *29*, 030601.
[13] A. Hooper, G. L. Fisher, K. Konstadinidis, D. Jung, H. Nguyen, R. Opila, R. W. Collins, N. Winograd, D. L. Allara, *J. Am. Chem. Soc.* **1999**, *121*, 8052.
[14] G. L. Fisher, A. V. Walker, A. E. Hooper, T. B. Tighe, K. B. Bahnck, H. T. Skriba, M. D. Reinard, B. C. Haynie, R. L. Opila, N. Winograd, D. L. Allara, *J. Am. Chem. Soc.* **2002**, *124*, 5528.
[15] A. V. Walker, T. B. Tighe, O. M. Cabarcos, M. D. Reinard, B. C. Haynie, S. Uppili, N. Winograd, D. L. Allara, *J. Am. Chem. Soc.* **2004**, *126*, 3954.
[16] G. Nagy, A. V. Walker, *J. Phys. Chem. B* **2006**, *110*, 12543.
[17] A. V. Walker, G. L. Fisher, A. E. Hooper, T. Tighe, R. L. Opila, N. Winograd, D. L. Allara, in *Metallization of Polymers 2*, (Ed. E. Sacher), Klewer Academic/Plenum, New York **2002**, p. 117.
[18] *Standard Test Methods for Measuring Adhesion by Tape Test (ASTM D3359-09e2)*, ASTM International, West Conshohocken, PA **2009**.
[19] M. A. Crouch, T. C. DeVore, *Chem. Mater.* **1996**, *8*, 32.
[20] M. C. Rhoten, T. C. DeVore, *Chem. Mater.* **1997**, *9*, 1757.
[21] M. W. Ross, T. C. DeVore, *J. Phys. Chem. A* **2008**, *112*, 6609.
[22] I. R. G. Ogilvie, V. J. Sieben, C. F. A. Floquet, R. Zmijan, M. C. Mowlem, H. Morgan, *J. Micromech. Microeng.* **2010**, *20*, 065016.
[23] G. Beamson, D. Briggs, *High Resolution XPS of Organic Polymers: the Scienta ESCA300 Database*, John Wiley & Sons, New York **1992**.
[24] P. M. T. M. V. Attekum, J. W. A. V. d. Velden, J. M. Trooster, *Inorg. Chem.* **1980**, *19*, 701.
[25] K. Kishi, S. Ikeda, *J. Phys. Chem.* **1974**, *78*, 107.
[26] *Handbook of Solvents* (Ed: J. Wypych), ChemTec, Toronto, ON **2001**.
[27] S. Bistac, J. Schultz, *Macromolecular Chemical Physics* **1997**, *198*, 531.
[28] A. Priimagi, G. Cavallo, A. Forni, M. Gorynsztejn–Leben, M. Kaivola, P. Metrangolo, R. Milani, A. Shishido, T. Pilati, G. Resnati, G. Terraneo, *Adv. Funct. Mater.* **2012**, *22*, 2572.
[29] U. Mayer, V. Gutmann, W. Gerger, *Monatsh. Chem.* **1975**, *106*, 1235.
[30] V. Gutmann, *Coord. Chem. Rev.* **1976**, *18*, 225.
[31] V. Gutmann, *Electrochim. Acta* **1976**, *21*, 661.
[32] C. Laurence, J.-F. Gal, *Lewis Basicity and Affinity Scales: Data and Measurement*, John Wiley & Sons, New York **2009**.
[33] A. V. Walker, T. B. Tighe, J. Stapleton, B. C. Haynie, S. Upilli, D. L. Allara, N. Winograd, *Appl. Phys. Lett.* **2004**, *84*, 4008.
[34] G. L. Fisher, A. E. Hooper, R. L. Opila, D. L. Allara, N. Winograd, *J. Phys. Chem. B* **2000**, *104*, 3267.
[35] P. Bebin, R. E. Prud'homme, *J. Polym. Sci., Part B* **2002**, *40*, 82.
[36] J. Spevacek, B. Schneider, *Adv. Colloid Interface Sci.* **1987**, *27*, 81.
[37] R. C. Estler, R. N. Zare, *Chem. Phys.* **1978**, *28*, 253.
[38] T. C. DeVore, J. L. Gole, *Chem. Phys.* **1993**, *174*, 409.
[39] *Handbook of Chemistry and Physics, 92nd. Ed., Internet version,* (Ed: W. M. Haynes), CRC Press, Boca Raton, FL **2012**, Ch. 9, p. 65.